B. Axial Developed Flow Between Concentric Cylinders

For this flow type, two cases were studied (the predicted values of C_f are shown in Table 1). For one typical flow at $a^+ = 21$ and $\delta/a = 11$, even close to the wall all of the models predict deviation in the mean velocity profile from that for the plane channel, in agreement with the DNS data (Fig. 5). The complete velocity profile computed by the low-Re k-ϵ RM model is in the best agreement with the DNS data. The Reynolds stress predicted by all of the models, except Chien's model, is also in very good agreement (almost coincident) with the DNS data. The four models (except Chien's model) accurately predict significant reduction in the Reynolds stress in the wall variables as compared with that for the plane channel (not shown here).

III. Discussion and Concluding Remarks

From the results presented in Sec. II it is clear that for the axial developed flow between concentric cylinders most models (except Chien's model) predict all quantities in reasonably good agreement with the DNS data. In contrast, for thick axisymmetric boundary layers at small a^+, the five models underpredict turbulence quantities and C_f by large amount.

To understand the difference in the predictions for the two flow configurations we need to consider the details of the flows. One difference between the two flow configurations is in the Reynolds number. Thick axisymmetric boundary layers are at a much higher Reynolds number as compared with that for the axial developed flow between concentric cylinders. Another possibility is that the measurements for the boundary-layer flow are in error because of the misalignment of the cylinder and/or because C_f is incorrectly deduced. Recently, Bull and Dekkars[13] have shown that in the boundary-layer flow at small radius Reynolds numbers (Re_a), even at about 1-deg yaw angle, vortex shedding from the cylinder may lead to additional turbulence generation. A third possibility is that the flow structure in the two cases is different. In the experiments on thick axisymmetric boundary layers,[7] large eddies scaling with the boundary-layer thickness have been observed to move across the cylinder. This is not accounted for in any of the models. This viscous-inviscid interaction is absent in DNS of axial developed flow between concentric cylinders.[11]

References

[1]Michelassi, V., Rodi, W., and Zhu, J., "Testing a Low Reynolds Number k-ϵ Turbulence Model Based on Direct Simulation Data," *AIAA Journal*, Vol. 31, No. 9, 1993, pp. 1720–1723.

[2]Rodi, W., Mansour, N. N., and Michelassi, V., "One-Equation Near-Wall Turbulence Modelling with the Aid of Direct Simulation Data," *Journal of Fluids Engineering*, Vol. 115, No. 2, 1993, pp. 196–205.

[3]Patel, V. C., Rodi, W., and Scheuerer, G., "Turbulence Models for Near-Wall and Low Reynolds Number Flows: A Review," *AIAA Journal*, Vol. 23, No. 9, 1985, pp. 1308–1318.

[4]Cebeci, T., "Laminar and Turbulent Incompressible Boundary Layers on Slender Bodies of Revolution in Axial Flow," *Journal of Basic Engineering*, Vol. 92, No. 3, 1970, pp. 545–554.

[5]Cebeci, T., "Eddy-Viscosity Distribution in Thick Axisymmetric Turbulent Boundary Layers," *Journal of Fluids Engineering*, Vol. 95, No. 2, 1973, pp. 319–326.

[6]Willmarth, W. W., Winkel, R. E., Sharma, L. K., and Bogar, T. J., "Axially Symmetric Turbulent Boundary Layers on Cylinders: Mean Velocity Profiles and Wall Pressure Fluctuations," *Journal of Fluid Mechanics*, Vol. 76, July 1976, pp. 35–64.

[7]Luxton, R. E., Bull, M. K., and Rajagopalan, S., "The Thick Turbulent Boundary Layer on a Long Cylinder in Axial Flow," *Aeronautical Journal*, Vol. 88, No. 875, 1984, pp. 186–199.

[8]Patel, V. C., "A Unified View of the Law of the Wall Using Mixing Length Theory," *Aeronautical Quarterly*, Vol. 24, No. 1, 1973, pp. 55–70.

[9]Denli, N., and Landweber, L., "Thick Axisymmetric Turbulent Boundary Layer on a Circular Cylinder," *Journal of Hydronautics*, Vol. 13, No. 3, 1979, pp. 92–104.

[10]Lueptow, R. M., Leehey, P., and Stellinger, T., "The Thick, Turbulent Boundary Layer on a Cylinder: Mean and Fluctuating Velocities," *Physics of Fluids*, Vol. 28, No. 12, 1985, pp. 3495–3505.

[11]Neves, J. C., Moin, P., and Moser, R. D., "Effects of Convex Transverse Curvature on Wall-Bounded Turbulence. Part 1. The Velocity and Vorticity," *Journal of Fluid Mechanics*, Vol. 272, Aug. 1994, pp. 349–381.

[12]Dewan, A., and Arakeri, J. H., "A Comparison of Four Turbulence Models for Wall-Bounded Flows Affected by Transverse Curvature," Dept. of Mechanical Engineering, Indian Inst. of Science, TR FM 1/95, Bangalore, India, Oct. 1995.

[13]Bull, M. K., and Dekkars, W. A., "Vortex Shedding from Long Slender Cylinders in Near-Axial Flow," *Physics of Fluids*, Vol. 5, No. 12, 1993, pp. 3296–3298.

Performance of Eddy-Viscosity-Based Turbulence Models in Three-Dimensional Turbulent Interaction

Datta Gaitonde* and J. S. Shang†
U.S. Air Force Wright Laboratory,
Wright–Patterson Air Force Base, Ohio 45433-7913
and
J. R. Edwards‡
North Carolina State University,
Raleigh, North Carolina 27695-7103

I. Introduction

In recent years, the numerical simulation of three-dimensional turbulent interactions has received considerable impetus from developments in two different areas: Riemann solvers and turbulence modeling. Sophisticated upwinded methods for the inviscid terms of the Navier–Stokes equations obviate the need for specification of arbitrary damping coefficients. Solvers employing such high-resolution flux evaluation techiques are superior to central-difference-based schemes not only in shock capturing but also in resolving smoother viscous-dominated regions of the flow.[1]

Advances in eddy-viscosity-based turbulence modeling have been reported principally in one- and two-equation formulations.[2–4] Although turbulence model development and evaluation efforts have focused on two-dimensional interactions, most practical flows are inherently three-dimensional. Fewer efforts have systematically investigated the performance of popular turbulence models in three-dimensional flows, where the physical processes are significantly different from those found in two dimensions.[5] This work examines several eddy-viscosity turbulence models for their ability to reproduce the experimental data in a strong three-dimensional external-shock-wave–turbulent-boundary-layer interaction. The four models investigated are the zero-equation Baldwin–Lomax (BL) model,[6] the one-equation models of Baldwin and Barth[2] (BB) and of Spalart and Allmaras[3] (SA), and the two-equation k–ϵ closure.[7]

The quantitative evaluation of turbulence models in three dimensions has been significantly aided by recent measurements not only of surface pressure but also of gradient quantities closely linked to the viscous and turbulent stresses. The error bounds on such data are typically less than 10%. The experimental geometries are simple, typically a combination of fins on a plate or cylinder–flare intersections. For fin-based configurations, computational results with zero- and two-equation models[8] indicate that good agreement is achieved with experimental data for surface pressure, perhaps as a consequence of the inviscid rotational nature of the dominant portion of the flowfield. However, the effort to match derivative quantities such as skin friction coefficients and heat transfer rates has proven to be considerably more challenging (see Ref. 9 for example).

Received July 26, 1995; revision received Nov. 8, 1995; accepted for publication Nov. 9, 1995.

*Visiting Scientist, Computational Fluid Dynamics Research Branch, Aeromechanics Division; also Scientist, UES, Inc., 4401 Dayton–Xenia Road, Dayton, OH 45432. Senior Member AIAA.

†Senior Scientist. Fellow AIAA.

‡Assistant Professor, Department of Mechanical and Aerospace Engineering. Member AIAA.

II. Results

The geometry of interest in the present work is a cylinder–flare juncture (Fig. 1) characteristic of an external flow situation. Detailed measurements of surface pressures and skin-friction coefficients have recently been reported.[10] The model is composed of a sting-supported cylinder forming a juncture with a 20-deg-half-angle conical flare. The principal region of interest—henceforth called the juncture region—is in the vicinity of the inner-cylinder–flare connection. The axis of the flare is parallel to that of the inner and outer cylinders, but offset vertically by a distance equal to one-fourth the diameter of the inner cylinder. The incoming flow is Mach 2.89 at zero angle of attack. This configuration is advantageous in two respects: 1) the availability of extensive experimental data,[10] including surface pressures, skin-friction coefficients, and surface streamline patterns permits detailed quantitative validation; and 2) the shock structure is observed experimentally to be steady under these conditions, thus eliminating an additional element of uncertainty in numerical simulation.

The three-dimensional compressible Navier–Stokes equations are solved in strong conservation form with mass-averaged variables in a curvilinear coordinate system. Details of the implementation and the formulations of the eddy viscosity models may be found in Ref. 11 and the references contained therein. The freestream flow parameters in the computations duplicate the experimentally measured values and are summarized in Fig. 1, where $\delta(=1.1$ cm) is the nominal height of the boundary layer entering the interaction. The wall is assumed to be at the adiabatic wall temperature of 262 K. The initial portion of the interaction, extending to a few boundary-layer thicknesses upstream of the juncture, is axisymmetric because of the geometry. To save resources, this portion is computed under the assumption of axisymmetry with only a few circumferential points. These results are then employed to provide a boundary-layer profile roughly 10δ upstream of the juncture by matching the experimental mean skin-friction coefficient of the incoming flow on the periphery of the inner cylinder.

The global Cartesian coordinate system is located at the juncture on the upper plane of symmetry. The subsequent discussion also employs the angle θ measured with respect to the cylinder axis. Thus $\theta = 0$ and 180 deg refer to the upper and lower symmetry planes, respectively. Since the configuration is symmetric, only one side of the symmetry plane is computed. To estimate solution dependence on mesh resolution, calculations are described on two meshes, designated M1 and M2. On each mesh, the point distribution is optimized to obtain increased resolution in the interaction region. M1 contains $113 \times 97 \times 89$ nodes and resolves the incoming boundary layer with 65 points; the corresponding figures for M2 are $113 \times 125 \times 115$ and 94. All turbulence models are computed on M1. Only the k–ϵ method, which requires the most stringent resolution criteria to be met, is investigated in M2. Both meshes satisfy the constraint of mean $y^+ < 1$ associated with the k–ϵ model.

At the upstream end of the domain, the incoming profiles of all necessary quantities are specified, including values of k^2/ϵ for the one-equation models and of k and ϵ for the two-equation model. Separate calculations are employed for this purpose, as outlined in the preceding section. At the downstream and far-field boundaries, the zero-gradient condition is specified. Spurious reflections are minimized by designing the meshes so that the shock system passes out of the domain at the downstream boundary. On the solid

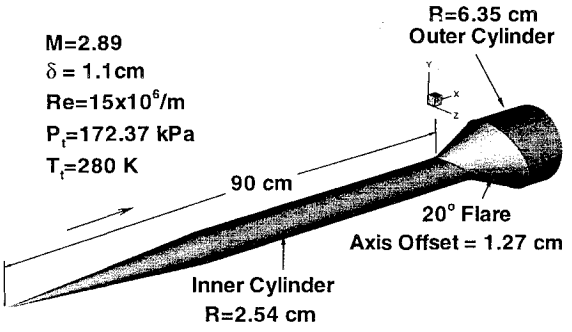

Fig. 1 Geometry of cylinder–offset-flare juncture.

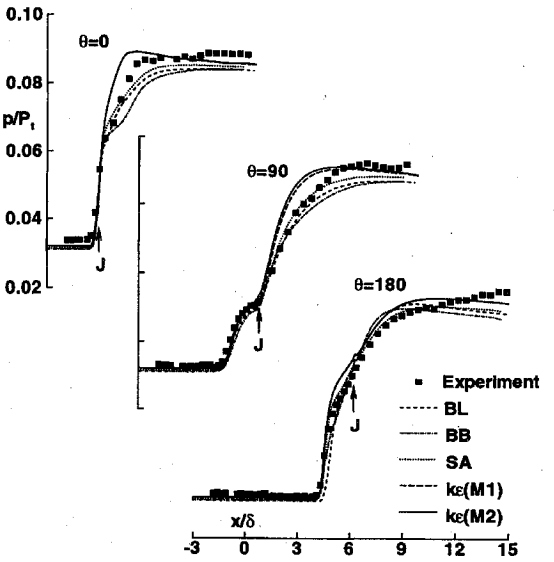

Fig. 2 Streamwise surface-pressure comparison at the upper and lower symmetry planes ($\theta = 0$, 180 deg) and at $\theta = 90$ deg. J = juncture location.

surface, no slip is assumed in conjunction with the zero normal pressure gradient and fixed adiabatic wall temperature, while symmetry is imposed on the upper and lower symmetry planes.

For brevity, some results are stated without accompanying figures, which may be found in Ref. 11. A systematic comparison of the computational capabilities, including the influence of mesh resolution, is presented by plotting the surface pressure and skin-friction coefficients along the three streamwise lines corresponding to the two symmetry planes $\theta = 0$ and 180 deg and along $\theta = 90$ deg.

Figure 2 displays the surface pressures at the three circumferential locations. The ordinate is the static pressure normalized by the upstream total pressure, and the abscissa is the streamwise distance normalized by the nominal boundary-layer thickness. The location of the juncture has been marked in each figure. Note that the domain plotted terminates at the flare–outer-cylinder intersection. Hence, the pressure drop associated with the corresponding expansion is not evident. The shock arising from the flare is conical in the inviscid regions away from the surface. The shock angle of roughly 31.5 deg is in good agreement with theory. Each method captures the shock in a very crisp fashion with a minimal amount of staircasing.

A measure of the upstream influence is defined by the location of the initial pressure rise. It is evident from Fig. 2 that this is very accurately computed by each of the methods. A similar conclusion is obtained upon comparison of the initial deflection of the surface skin-friction vector (not shown). The rate of pressure rise in the inception region of the interaction up to the juncture is also correctly estimated. Beyond the juncture location, however, several differences are evident. The BB method predicts a lower rate of pressure rise than the other methods, thus resulting in underprediction of the peak pressure. In contrast, with the k–ϵ method, the pressure rises more rapidly to its asymptote as a consequence of a slightly smaller predicted interaction region. On each of the sections however, the pressure is modestly underpredicted in the trailing portion of the region plotted, i.e., in the vicinity of the flare–outer-cylinder intersection. The largest discrepancy in the downstream region occurs on the lower plane of symmetry with the BB method (8%); the best comparison is shown by the k–ϵ scheme (3%).

The plateau region of the pressure profile, characteristic of swept interactions, is not pronounced on the symmetry planes but is conspicuous on the $\theta = 90$-deg line near the juncture, where there is significant crossflow. This plateau is evident in the results by each closure. Proceeding around the periphery, an increase is observed in the spanwise extent over which the pressure rise occurs. Overall, the computational results accurately predict the trend of experimental pressure data, and in the interaction region the discrepancy is relatively small. An examination of all plots in Fig. 2 demonstrates that the degree of mesh resolution with M1 is adequate in this regard. The maximum variation in pressure is only about 1% and is observed at $\theta = 90$-deg downstream of the juncture ($x/\delta \approx 7$).

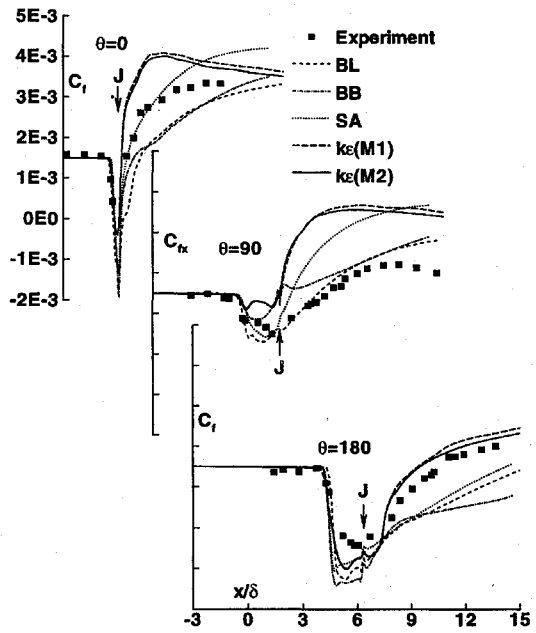

Fig. 3 Comparison of skin-friction coefficient at the upper and lower symmetry planes ($\theta = 0, 180$ deg) and at $\theta = 90$ deg. J = juncture location.

Figure 3 compares the computed skin-friction coefficient distributions with the measured data at the three azimuthal angles. Because of the matching procedure employed, the values agree reasonably in the upstream region of the undisturbed boundary layer. At each angle, the skin-friction value drops to reach a minimum before showing the rapid recovery typical of postattachment flow. On both planes of symmetry, the skin friction becomes negative, indicating separation of the incoming boundary layer and associated reversed flow.

The region of separation is small at $\theta = 0$ compared to that at $\theta = 180$ deg. This is consistent with the observation made earlier in relation to Fig. 2—the size of the interaction increases in every respect with the azimuthal angle θ in proximity to the upper symmetry plane. This greater domain of interaction is a consequence of fluid movement from the upper to the lower symmetry plane. The recovery of C_f subsequent to attachment is also more rapid on the upper symmetry plane, where the separated region is smaller and the peak skin friction reaches a much higher value, about 3 times that in the incoming boundary layer. Both the BL and BB methods predict a more gradual rise and thus underpredict C_f in regions downstream of attachment. In contrast, the Spalart–Allmaras model displays the correct rate of rise but fails to predict the leveling off observed in the region $x/\delta \approx 5$. The k–ϵ method predicts a more rapid rise of skin friction than in experiment, but successfully captures the asymptote of skin friction in the downstream regions.

On the lower plane of symmetry ($\theta = 180$ deg in Fig. 3), the peak skin-friction coefficient is only about twice the upstream value and occurs near the outer-cylinder juncture. All methods reproduce the point of separation accurately. However, a common trend is reflected in the overprediction of the near-wall backflow velocity magnitude, manifested by a lower backflow skin-friction level (i.e., higher negative magnitude) than observed experimentally. All methods also show a small spike near the juncture location, where a slope discontinuity exists. Nevertheless, the k–ϵ method performs considerably better in this region than the other methods, the C_f predictions being within 10% of the experimental value over the entire domain length.

At $\theta = 90$ deg, the comparison between experiment and data deteriorates, with all methods displaying significant overprediction of skin-friction values. Note that the x component of C_f is plotted here. The two methods that provide better results on the symmetry planes (i.e., k–ϵ and SA) are the worst at this location. Although the BB and BL methods appear to be more accurate in this region, the good agreement may be fortuitous in view of the tendency of these methods to underpredict the recovery of C_f on the upper and lower symmetry planes. In general, the calculations indicate more sensitivity to mesh resolution for C_f than for pressure. The variation in C_f is nevertheless restricted to the region downstream of attachment, and the maximum change is less than 3%.

Some of the C_f data trends on the symmetry planes may be compared with those observed in two-dimensional or axisymmetric situations. For axially separated two-dimensional flows, the SA and BB models induce a rather slow velocity recovery downstream of reattachment,[12] resulting in an underprediction of C_f. A similar trend occurs for the three-dimensional separation at $\theta = 180$ deg. The overly rapid recovery of C_f with the two-equation model has also been observed in earlier work.[4] The cause suggested in Ref. 4 is that there is an abnormal collapse of ϵ near attachment leading to strong growth in length scale. This source of error is not present in the zero- and one-equation models, in which the length scale is specified, and its effect on the overall results is minor.

The failure to reproduce C_f values in regions of significant crossflow may be traced to assumptions inherent in the formulation. In contrast to that at $\theta = 0$ and 180 deg, the flow at $\theta = 90$ deg is characterized by a large degree of three-dimensionality in the presence of a pressure gradient. It is noted in Ref. 5 that turbulence models extrapolated from two-dimensional experience miss some essential features of three-dimensional flows. The example discussed in Ref. 5 specifically deals with the effect of crossflow pressure gradient, such as exists in the present configuration, and its resultant anomalous effects, which affect the development of and relationships between mean shear stresses and the corresponding strain rates. Scalar eddy-viscosity-based solutions, however, are pseudolaminar and impose a close relationship between the stresses and the mean-flow gradients; thus they may not be very accurate away from the flows for which they have been calibrated.[13]

These characteristics of the comparison between theory and experiment bear resemblance to results on other three-dimensional shock-wave–turbulent-boundary-layer interactions. In particular, in Ref. 8 both the BL and k–ϵ models were investigated for the crossing-shock or double-fin configuration. Those results indicated similarly good results for all features, particularly with the k–ϵ model, except for C_f in regions of large crossflow occurring after attachment. A comparison with flowfield surveys of pitot pressure indicated that the vortical structure caused by the interaction is accurately reproduced.[8] The properties of the primary vortical structure are dependent upon those of the upstream fully developed boundary layer and the shock wave, both of which are accurately represented by the turbulence model and the inviscid discretization, respectively, as is their interaction. Within the interaction region, inadequacies in turbulence modeling influence principally the complex mechanisms in the flow close to the wall, which affect the development of the turbulent stresses. For the double fin, therefore, the generally accepted conclusion in the literature (see Ref. 8 and the references therein) is that the primary vortical structure is predominantly inviscid and rotational. The parallel situation with regard to validation in the present configuration indicates that a similar conclusion may be appropriate here for the major features of the vortical structure. This conjecture must be verified by comparisons with off-surface flowfield quantities.

III. Summary

The performance of a hierarchy of popular turbulence models in a three-dimensional external-shock-wave–turbulent-boundary-layer interaction caused by a cylinder–offset-flare juncture has been investigated. The turbulence closures examined are the zero-equation BL algorithm, the one-equation models of BB and of SA, and a variant of the two-equation k–ϵ method. The influence of mesh resolution has been examined. All methods reproduce the theoretical shock structure and the experimentally measured upstream influence. With minor variations, the surface pressures are well obtained in all regions. The performance for the surface skin-friction coefficient, however, requires qualification. Each method predicts the C_f profile in some regions, and in each region at least one method may be deemed accurate. However, no one model performs well everywhere. Overall, the SA and k–ϵ models exhibit similar properties and are modestly more accurate than the BL and BB methods.

Acknowledgments

The authors thank James L. Brown for making the experimental data available in a convenient and timely fashion. This work was supported in part by a grant of high-performance computing (HPC)

time from the HPC Department of Defense Shared Resource Center, U.S. Army Corps of Engineers Waterways Experiment Station, Vicksburg, MS, as well as from the Numerical Aerodynamic Simulation facility.

References

[1]Allmaras, S. R., "Contamination of Laminar Boundary Layers by Artificial Dissipation in Navier–Stokes Solutions," Annual Modeling and Simulation Conf., Pittsburgh, PA, April 1992.

[2]Baldwin, B. S., and Barth, T. J., "A One-Equation Turbulence Transport Model for High Reynolds Number Wall-Bounded Flows," AIAA Paper 91-0610, Jan. 1991.

[3]Spalart, P. R., and Allmaras, S. R., "A One-Equation Turbulence Model for Aerodynamic Flows," AIAA Paper 92-0439, Jan. 1992.

[4]Coakley, T. J., and Huang, P. G., "Turbulence Modeling for High Speed Flows," AIAA Paper 92-0436, Jan. 1992.

[5]Bradshaw, P., "Progress in Turbulence Research," AIAA Paper 90-1480, June 1990.

[6]Baldwin, B. S., and Lomax, H., "Thin Layer Approximation and Algebraic Model for Separated Turbulent Flows," AIAA Paper 78-0257, Jan. 1978.

[7]Launder, B. E., and Sharma, B. I., "Application of the Energy Dissipation Model of Turbulence to the Calculation of Flows Near a Spinning Disk," *Letters in Heat and Mass Transfer*, Vol. 1, 1974, pp. 131–138.

[8]Gaitonde, D., and Shang, J. S., "The Structure of a Double-Fin Turbulent Interaction at Mach 4," AIAA Paper 94-2810, June 1994; *AIAA Journal* (to be published).

[9]Gaitonde, D., and Shang, J. S., "On the Structure of an Unsteady Type IV Interaction at March 8," *Computers and Fluids Journal*, Vol. 24, No. 4, 1995, pp. 469–485.

[10]Wideman, J. K., Brown, J. L., Miles, J. B., and Özcan, O., "Skin-Friction Measurements in a Three-Dimensional, Supersonic Shock-Wave/Boundary-Layer Interaction," *AIAA Journal*, Vol. 33, No. 5, 1995, pp. 805–811.

[11]Gaitonde, D., Edwards, J. R., and Shang, J. S., "The Computed Structure of a 3-D Turbulent Interaction Caused by a Cylinder/Offset Flare Juncture," AIAA Paper 95-0230, Jan. 1995.

[12]Edwards, J. R., and Chandra, S., "Eddy Viscosity—Transport Turbulence Models for High-Speed, Two-Dimensional, Shock-Separated Flowfields," AIAA Paper 94-0310, Jan. 1994.

[13]Bradshaw, P., "Turbulence: The Chief Outstanding Difficulty of Our Subject," *Experiments in Fluids*, Vol. 16, 1994, pp. 203–216.

Skewed Shear-Layer Mixing Within a Duct

Thomas F. Fric*
General Electric Corporate R&D Center, Schenectady, New York 12301

Introduction

CASES occur where shear layers are inherently more three-dimensional than nominally two-dimensional mixing layers. The skewed mixing layer, which is formed by two streams at an angle to each other, is one example. Skewed mixing layers can be better mixers than two-dimensional layers,[1–4] and the analysis of Lu and Lele showed that the growth rate of skewed mixing layers can be represented by an effective shear-velocity difference of the two streams.[3]

In the experiments highlighted here, incompressible skewed shear-layer mixing is studied. The mixing region is confined in the sense that the streams impinge somewhat on the side walls of the duct into which the two streams flow. Generally there are differences in the two streams' relative speeds in both the streamwise and spanwise directions, and therefore fluxes of two vorticity components separate from the splitter plate. The mass flow ratio is varied for a fixed amount of skewing, and mixing development within the duct is investigated.

Received Nov. 28, 1994; presented as Paper 95-0869 at the AIAA 33rd Aerospace Sciences Meeting, Reno, NV, Jan. 9–12, 1995; revision received Oct. 27, 1995; accepted for publication Nov. 16, 1995.

*Aeronautical Engineer, Fluid Mechanics Program.

Experimental Setup

Figure 1 shows the two skewed streams, mixing duct, and laser, optics, and camera for the planar laser-induced fluorescence (PLIF) technique. The top and bottom streams are injected at 26 and 13 deg relative to the duct axis, respectively. The splitter-plate trailing edge is located 2.5 cm downstream of the transition between the injected streams and mixing duct. Screens and honeycomb were used to condition the injected streams. The distance from the downstream edge of each stream's flow conditioning to the splitter-plate edge was 47.0 cm, and the boundary-layer momentum thicknesses at the end of the splitter plate were estimated to be in the range of 0.5–1.1 cm, depending upon the mass flow rate. The mixing-duct dimensions are 12.7 cm wide by 9.3 cm high. Further details about the setup are available.[4]

Planar laser-induced fluorescence of fluorescein dye in water was used. All images captured by an 8-bit charge-coupled device (CCD) camera were corrected for laser sheet nonuniformity, background light, and camera response.[5] The laser sheet was steered across the mixing region to reveal cross-sectional images at several duct planes. The CCD camera viewed the mixing process through a window located at the end of the duct, 66.0 cm downstream from the splitter-plate trailing edge.

Table 1 shows flow conditions for five test cases. The bottom-to-top stream mass-flow ratio k defines each test case. High- and low-speed streams are indicated as streams 1 and 2, respectively. By ϕ_1 we denote the skewing angle of the higher-speed stream, and by ϕ_2 the skewing angle of the lower-speed stream, both relative to the duct axis. The total skewness ϕ is given by $\phi_2 - \phi_1$. The Reynolds number, based on duct height h and mean streamwise duct velocity, is 3000.

Results

Figure 2 show streamwise progression of mixing for $k = 2$. Each image shows time-averaged scalar concentrations of 50 instantaneous fields. The gray scale from white (top stream) to black (bottom stream) shows mixture levels between the two streams. At $x/h = 1$, Fig. 2a shows the growth and structure of the interface between the two streams and a counterclockwise rotation of the interface. The thin central portion of the shear layer shows evidence of two streamwise structures with counterclockwise vortical sense, and the bottom left and top right corners show the collection of streamwise vorticity. The top stream fluid, with a velocity component from right to left, impinges on the left duct wall and moves downward. Similarly the bottom stream fluid impinges on the right wall and moves upward, displacing what was initially pure top-stream fluid. Figure 2b shows mixing-layer growth and improvement in mixture uniformity at $x/h = 2$. Figures 2c and 2d show further development

Table 1 Flow conditions

$k \equiv m_b/m_t$	$r \equiv u_2/u_1$	ϕ_1, deg	ϕ_2, deg	$\phi \equiv \phi_2 - \phi_1$, deg
5	0.22	−13	26	39
2	0.54	−13	26	39
1	0.92	−13	26	39
0.5	0.46	26	−13	−39
0.2	0.18	26	−13	−39

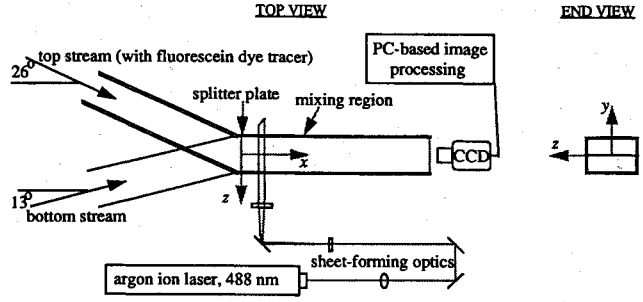

Fig. 1 Schematic of experimental setup.